Modulation transfer spectroscopy for ^{87}Rb atoms: theory and experiment

Heung-Ryoul Noh,[1,4] Sang Eon Park,[2,5] Long Zhe Li,[2,3] Jong-Dae Park,[3,*] and Chang-Ho Cho[3]

[1]*Department of Physics, Chonnam National University, Gwangju 500-757, Korea*
[2]*Korea Research Institute of Standards and Science, Daejeon 305-340, Korea*
[3]*Department of Physics, Paichai University, Daejeon 302-735, Korea*
[4]*hrnoh@chonnam.ac.kr*
[5]*parkse@kriss.re.kr*
[*]*jdpark@pcu.ac.kr*

Abstract: We conducted a theoretical and experimental study of lineshape in modulation transfer spectroscopy for ^{87}Rb atoms. When a linearly polarized pump beam, modulated at an angular frequency of Ω, overlaps in parallel with an unmodulated linearly polarized probe beam, combined modulated probe beams are generated via nonlinear interaction with atoms. The detected modulation transfer signals are calculated by numerically solving the complete optical Bloch equations for the ^{87}Rb atoms without the use of any phenomenological parameters. We find that the calculated results are in good agreement with experimental results.

OCIS codes: (020.1670) Coherent optical effects; (020.2930) Hyperfine structure; (020.3690) Line shapes and shifts.

References and links

1. W. Demtröder, *Laser Spectroscopy* (Springer, Berlin, 1998).
2. C. Wieman and T. W. Hänsch, "Doppler-free laser polarization spectroscopy," Phys. Rev. Lett. **36**(20), 1170–1173 (1976).
3. K. L. Corwin, Z. Lu, C. F. Hand, R. J. Epstein, and C. E. Wieman, "Frequency-stabilized diode laser with the Zeeman shift in an atomic vapor," Appl. Opt. **37**(15), 3295–3298 (1998).
4. M. L. Harris, S. L. Cornish, A. Tripathi, and I. G. Hughes, "Optimization of sub-Doppler DAVLL on the rubidium D2 line," J. Phys. B, **41**(8), 085401 (2008).
5. G. C. Bjorklund, "Frequency-modulation spectroscopy: a new method for measuring weak absorptions and dispersions," Opt. Lett. **5**(1), 15–17 (1980).
6. J. H. Shirley, "Modulation transfer processes in optical heterodyne saturation spectroscopy," Opt. Lett. **7**(11), 537–539 (1982).
7. D. J. McCarron, S. A. King, and S. L. Cornish, "Modulation transfer spectroscopy in atomic rubidium," Meas. Sci. Technol. **19**(10), 105601 (2008).
8. M. L. Eickhoff and J. L. Hall, "Optical frequency standard at 532 nm," IEEE Trans. Instrum. Meas. **44**(2), 155–158 (1995).
9. E. B. Kim, S. E. Park, C. Y. Park, Y. H. Park, D.-S. Yee, T. Y. Kwon, H. S. Lee, and H. Cho, "Absolute frequency measurement of $F = 4 \rightarrow F' = 5$ transition line of cesium using amplified optical frequency comb," IEEE Trans. Instrum. Meas. **56**(2), 448–452 (2007).
10. A. Schenzle, R. G. DeVoe, and R. G. Brewer, "Phase-modulation laser spectroscopy," Phys. Rev. A **25**(5), 2606–2621 (1982).
11. E. Jaatinen, "Theoretical determination of maximum signal levels obtainable with modulation transfer spectroscopy," Opt. Commun. **120**(1–2), 91–97 (1995).
12. F. Bertinetto, P. Cordiale, G. Galzerano, and E. Bava, "Frequency stabilization of DBR diode laser against Cs absorption lines at 852 nm using the modulation transfer method," IEEE Trans. Instrum. Meas. **50**(2), 490–492 (2001).

#153748 - $15.00 USD Received 30 Aug 2011; revised 5 Oct 2011; accepted 5 Oct 2011; published 2 Nov 2011

13. J. Zhang, D. Wei, C. Xie, and K. Peng, "Characteristics of absorption and dispersion for rubidium D2 lines with the modulation transfer spectrum," Opt. Express, **11**(11), 1338–1344 (2003).
14. L. Z. Li, S. E. Park, H. R. Noh, J. D. Park, and C. H. Cho, "Modulation transfer spectroscopy for a two-level atomic system with a non-cycling transition," J. Phys. Soc. Jpn. **80**(7), 074301 (2011).
15. A. R. Edmonds, *Angular Momentum in Quantum Mechanics* (Princeton University Press, Princeton, 1960).
16. J. Sagle, R. K. Namiotka, and J. Huennekens, "Measurement and modelling of intensity dependent absorption and transit relaxation on the cesium D_1 line," J. Phys. B **29**(12), 2629–2643 (1996).
17. P. Siddons, C. S. Adams, C. Ge, and I. G. Hughes, "Absolute absorption on rubidium D lines: comparison between theory and experiment," J. Phys. B **41**(15), 155004 (2008).

1. Introduction

The coherent interaction of laser light with atoms has drawn considerable interest since the advent of the laser. In particular, high resolution spectroscopy using tunable lasers has been developed to obtain sub-Doppler resolution in Doppler broadened atomic vapor cells [1]. Well-known sub-Doppler spectroscopies such as saturated absorption spectroscopy (SAS) [1] and polarization spectroscopy (PS) [2] are widely used in active laser frequency stabilization. From the perspective of laser frequency locking, in addition to the two methods mentioned above, there exists other methods such as dichroic atomic vapor laser lock (DAVLL) [3], sub-Doppler DAVLL [4], frequency modulation (FM) spectroscopy [5], and modulation transfer spectroscopy (MTS) [6, 7].

Of these methods, there has been considerable attention given to MTS due to its ability to provide robust laser frequency stabilization [8, 9]. As shown in Fig. 1(a), in MTS, the pump beam is frequency modulated, whereas the counter-propagating probe beam is not modulated. When two beams overlap in a vapor cell, new probe beams modulated at the frequency of $\omega \pm \Omega$ are generated, where ω and Ω are the laser frequency and modulation frequency, respectively. By beating these generated signals with the original probe beam, MTS signals oscillating in phase or in quadrature with the probe beams are created. Because the MTS signals exhibit dispersive lineshapes, they can be used in active frequency stabilization of the laser. One of the most important advantages of MTS is the fact that the operation is not sensitive to experimental conditions, such as temperature, because there is no linear background absorption involved. In addition, the MTS signal is significant only in the cycling transitions. These characteristics become very important when the frequency spacings of the excited states are very small.

After the initial report on the MTS was published [6], there were many papers on MTS from both theoretical and experimental points of view [7–13]. Recently Li *et al.* proved that MTS signals were suppressed significantly for open transitions by calculating the MTS signals for open two-level atoms [14]. In the case of real atoms, even though there are many reports on practical experiments, to the best of our knowledge, there are no reports on the accurate theoretical calculation of the MTS spectrum. In this paper, we present a theoretical and experimental study of the MTS spectrum for ^{87}Rb atoms where a modulated pump and an unmodulated probe beam counter propagate and are linearly polarized in parallel. The method described in this paper can be used in calculating the signals for other atoms and in other polarization configurations.

The paper is structured as follows. Section 2 describes the theory used to calculate the MTS signals for ^{87}Rb atoms. Experimental methods are presented in Sec. 3. The calculated and experimental results of the MTS spectra are reported in Sec. 4 and a summary is presented in the final section.

2. Theory

The energy level diagram of a ^{87}Rb atom used for calculating the MTS spectrum is shown in Fig. 1(b). The linearly polarized pump and probe beams are tuned to the transitions $F_g \rightarrow F_e = F_g - 1, F_g, F_g + 1$, where $F_g = 1$ or 2. We calculated the internal dynamics of a ^{87}Rb atom using

#153748 - $15.00 USD Received 30 Aug 2011; revised 5 Oct 2011; accepted 5 Oct 2011; published 2 Nov 2011

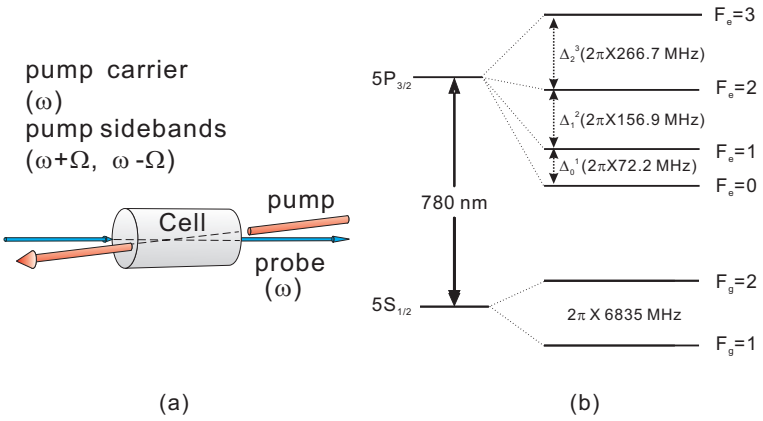

Fig. 1. (a) Schematic diagram of modulation transfer spectroscopy. (b) Energy level diagram of ^{87}Rb atom.

a following density-matrix equation:

$$\dot{\rho} = -(i/\hbar)\,[H_0 + V, \rho] + \dot{\rho}_{\rm sp}, \tag{1}$$

where ρ is the density operator. The bare atomic Hamiltonian, H_0, is given by

$$H_0 = \sum_{F_e=F_g-1}^{F_g+1} \sum_{m_e=-F_e}^{F_e} \hbar(\omega_0 - \Delta_{F_e}^{F_g+1}) \left|F_e, m_e\right\rangle \left\langle F_e, m_e\right|, \tag{2}$$

where ω_0 is the resonant frequency between the excited state $\left|F_e = F_g + 1\right\rangle$ and the ground state $\left|F_g\right\rangle$ and Δ_ν^μ is the frequency difference between $|F_e = \mu\rangle$ and $|F_e = \nu\rangle$ ($\mu \geq \nu$). Since the pump beam is frequency modulated whereas the probe beam is not modulated, the interaction Hamiltonian can be explicitly written as

$$\begin{aligned} V = \sum_{F_e=F_g-1}^{F_g} \sum_{m=-F_g}^{F_g} \frac{\hbar}{2} C_{F_g,m}^{F_e,m} \Big(& \Omega_c e^{-i\omega_1 t} + \Omega_s e^{-i(\omega_1+\Omega)t} \\ & - \Omega_s e^{-i(\omega_1-\Omega)t} + \Omega_p e^{-i\omega_2 t} \Big) \left|F_e, m\right\rangle \left\langle F_g, m\right| + h.c., \end{aligned} \tag{3}$$

where Ω_c, Ω_s, and Ω_p are the Rabi frequencies of the carrier, sideband, and probe beams. *h.c.* implies hermitian conjugate. In Eq. (3), $C_{F_g,m_g}^{F_e,m_e}$ is the normalized transition strength between the states $|F_e, m_e\rangle$ and $\left|F_g, m_g\right\rangle$, and is given by [15]

$$\begin{aligned} C_{F_g,m_g}^{F_e,m_e} &= (-1)^{2F_e+I+J_g+J_e+L_g+S+m_{F_g}+1} \\ &\quad \times \sqrt{(2L_e+1)(2J_e+1)(2J_g+1)(2F_e+1)(2F_g+1)} \\ &\quad \times \left\{ \begin{array}{ccc} L_g & L_e & 1 \\ J_e & J_g & S \end{array} \right\} \left\{ \begin{array}{ccc} J_g & J_e & 1 \\ F_e & F_g & I \end{array} \right\} \left(\begin{array}{ccc} F_e & 1 & F_g \\ m_e & m_g - m_e & -m_g \end{array} \right), \end{aligned}$$

where L, S, and I represent the orbital, electron spin, and nuclear spin angular momenta, respectively. $(\cdots)$ and $\{\cdots\}$ denote the $3J$ and $6J$ symbols, respectively. In Eq. (3), $\omega_1 = \omega + kv$ and $\omega_2 = \omega - kv$ are the laser frequencies of the carrier pump and the probe beam in the rest frame of an atom moving with velocity v where $k = \omega/c$ is the wave vector.

#153748 - $15.00 USD Received 30 Aug 2011; revised 5 Oct 2011; accepted 5 Oct 2011; published 2 Nov 2011

In Eq. (1), $\dot{\rho}_{\rm sp}$ is the spontaneous emission term whose matrix elements are given by

$$\begin{aligned}
\langle F_e,m|\,\dot{\rho}_{\rm sp}\,|F_e',m'\rangle &= -\Gamma\langle F_e,m|\,\rho\,|F_e',m'\rangle,\\
\langle F_e,m|\,\dot{\rho}_{\rm sp}\,|F_g,m'\rangle &= -(\Gamma/2)\langle F_e,m|\,\rho\,|F_g,m'\rangle,\\
\langle F_g,m|\,\dot{\rho}_{\rm sp}\,|F_g,m'\rangle &= \Gamma\sum_{F_e=F_g-1}^{F_g+1}\sum_{q=-1}^{1}C_{F_g,m}^{F_e,m+q}C_{F_g,m'}^{F_e,m'+q}\langle F_g,m|\,\rho\,|F_g,m'\rangle,
\end{aligned}\tag{4}$$

where Γ is the decay rate of the excited state and $\left(\dot{\rho}_{\rm sp}\right)_{ij}=\left(\dot{\rho}_{\rm sp}\right)_{ji}$ for $i\neq j$. Fast time dependence of the density matrix equation (Eq. (1)) is eliminated by using slowly varying variables, defined as $\rho_{ij}=e^{c_{ij}t}\sigma_{ij}$ where $c_{ij}=-(+)\omega$ for i and j which denotes the excited (ground) and ground (excited) states, respectively. $c_{ij}=0$ for both i and j denoting the excited or ground states. Then, Eq. (1) can be transformed into the following equation:

$$\dot{\sigma}_{ij}=e^{-ic_{ij}t}\dot{\rho}_{ij}-ic_{ij}\sigma_{ij},\tag{5}$$

where $\dot{\rho}_{ij}$ is the matrix element from Eq. (1).

As σ_{ij} possesses explicit time dependence, it is necessary to know the oscillation frequencies. Since all the carrier, sideband, and probe beams of frequency ω_1, $\omega_1\pm\Omega$, and ω_2, respectively, are linearly polarized in parallel, all the frequencies are coupled with each other. There exist optical coherences connecting the excited and ground states with equal magnetic quantum numbers, and all other coherences vanish. When we consider the interactions of up to three photons, as reported in the previous paper on two-level atoms [14], the populations have 11 oscillation frequencies [0, $\pm\Omega$, $\pm2\Omega$, $\pm\delta_{\rm p}$, $\pm\left(\delta_{\rm p}+\Omega\right)$, and $\pm\left(\delta_{\rm p}-\Omega\right)$] whereas the excited–ground state coherences have 20 oscillation frequencies [0, $-\delta_{\rm p}$, $-\delta_{\rm p}\pm\Omega$, $-\delta_{\rm p}\pm2\Omega$, $\delta_{\rm p}$, $\delta_{\rm p}\pm\Omega$, $\delta_{\rm p}\pm2\Omega$, $-2\delta_{\rm p}$, $-2\delta_{\rm p}\pm\Omega$, $\pm\Omega$, $\pm2\Omega$, and $\pm3\Omega$], where $\delta_{\rm p}=\omega_2-\omega_1=-2kv$. For use later, we define new variables, the detunings $\delta=\omega-\omega_0$ and $\delta_1=\delta+kv$. Of the oscillation frequencies for the populations, 0, $\pm\Omega$, and $\pm2\Omega$ denote the emission and absorption of two carrier photons, one carrier and one sideband photon, and two sideband photons, respectively. The remaining oscillation frequencies can be understood in a similar way.

In order to simplify our calculations, in this paper we consider only the oscillation frequencies 0 and $\pm\Omega$, not all 11 frequencies mentioned above [14]. In fact, the oscillation frequency 0 corresponds to the interaction of two carrier photons, whereas $\pm\Omega$ corresponds to the interaction of a carrier photon and a sideband photon. This is validated by the numerical calculation shown in Sec. 4. This approximation can also be understood as follows; when the probe photon is neglected, the populations can be thought of as generated via a two-photon interaction of the carrier and sideband photons. The probe photon then contributes to the optical coherences via three-photon interactions. Therefore, we have five oscillation frequencies for the populations: 0, $\pm\Omega$, and $\pm2\Omega$. By assuming a weak sideband intensity, we can ignore the frequency $\pm2\Omega$. Accordingly, the excited-ground state coherences have the oscillation frequencies $-\delta_{\rm p}\pm\Omega$, $-\delta_{\rm p}$, 0, $\pm\Omega$, and $\pm2\Omega$. The validity of this approximation will be discussed later. The oscillation frequencies of the ground-excited state coherences have the opposite sign to those of the excited-ground state coherences. The explicit expression of the population is given by the following:

$$\sigma_{jj}=p_{jj1}+\left(p_{jj2}+ip_{jj3}\right)e^{-i\Omega t}+\left(p_{jj2}-ip_{jj3}\right)e^{i\Omega t},\tag{6}$$

where j runs over all magnetic sublevels, whereas the coherences are given by

$$\begin{aligned}
\sigma_{ij} &= \left(r_{ij1}+is_{ij1}\right)e^{i\left(-\delta_{\rm p}-\Omega\right)t}+\left(r_{ij2}+is_{ij2}\right)e^{i\left(-\delta_{\rm p}+\Omega\right)t}\\
&\quad+\left(r_{ij3}+is_{ij3}\right)e^{-i\delta_{\rm p}t}+\text{other 5 terms},
\end{aligned}\tag{7}$$

#153748 - $15.00 USD Received 30 Aug 2011; revised 5 Oct 2011; accepted 5 Oct 2011; published 2 Nov 2011

where i and j represent the excited and the ground states, respectively.

Inserting Eqs. (6) and (7) into Eq. (5), we get a set of coupled differential equations. These equations can then be solved numerically as a function of time, δ_1, and δ_p. As described in a previous report [14], the detected signal can be calculated from the induced dipole moment as given by

$$\begin{aligned}\langle d\rangle &= \mathrm{Tr}(\rho d) = d_{eg}\sum_{ij} C_{ij}\left\{\left(r_{ij1}+is_{ij1}\right)e^{i(-\omega_2-\Omega)t}+\left(r_{ij2}+is_{ij2}\right)e^{i(-\omega_2+\Omega)t}\right.\\ &\left.+\left(r_{ij3}+is_{ij3}\right)e^{-i\omega_2 t}+\text{other 5 terms}+c.c\right\},\end{aligned} \tag{8}$$

where i and j run over the excited and ground states, respectively. C_{ij} is the relative transition strength between the states i and j. Since the electric field generated from the oscillating dipole in Eq. (8) is shifted in phase by $\pi/2$, the detected signals resulting from the beating of the generated electric field with the probe field are given by

$$I_0(\delta_1,\delta_p,t)\cos\Omega t + Q_0(\delta_1,\delta_p,t)\sin\Omega t,$$

where I_0 and Q_0 are the in-phase and quadrature phase components of the detected signal, respectively, and are given by

$$\begin{aligned} I_0(\delta_1,\delta_p,t) &= \sum_{ij} C_{ij}\left(s_{ij2}+s_{ij1}\right),\\ Q_0(\delta_1,\delta_p,t) &= \sum_{ij} C_{ij}\left(r_{ij2}-r_{ij1}\right),\end{aligned} \tag{9}$$

respectively.

The in-phase and quadrature components are then averaged over the transverse and longitudinal velocity distributions, and the final results are given by

$$\begin{aligned} I &= \frac{1}{t_{\mathrm{av}}}\int_0^{t_{\mathrm{av}}} \mathrm{d}t \int_{-\infty}^{\infty} \mathrm{d}v\, f_{\mathrm{D}}(v) I_0(\delta+kv,-2kv,t)\\ Q &= \frac{1}{t_{\mathrm{av}}}\int_0^{t_{\mathrm{av}}} \mathrm{d}t \int_{-\infty}^{\infty} \mathrm{d}v\, f_{\mathrm{D}}(v) Q_0(\delta+kv,-2kv,t),\end{aligned} \tag{10}$$

where

$$f_{\mathrm{D}} = \left(\sqrt{\pi}u\right)^{-1}\exp\left[-(v/u)^2\right]$$

is the Maxwell-Boltzmann velocity distribution function. $u(=(2k_BT/M)^{1/2})$ is the most probable speed (T: temperature of the cell, M: mass of an atom) and $t_{\mathrm{av}}(=(\sqrt{\pi}/2)d/u)$ is the average transit time to cross a laser beam of diameter d [16].

3. Experimental methods

We briefly describe experimental methods of MTS for ^{87}Rb atoms. We use a home-made ECDL (external-cavity diode laser) operating at 780 nm. A part of the laser beam is coupled into a polarization maintained fiber to get a Gaussian spatial beam profile. After spatial mode filtering, the laser beam is divided into two with a beam splitter. The transmitted beam goes into the Rb vapor cell which is surrounded by μ-metal film to reduce unwanted strong magnetic field produced by an optical isolator and magnetic post bases. The reflected beam is phase modulated at 3 MHz by a resonant-type electro optic modulator (EOM; Newfocus model 4001). The beam diameters of the pump and probe beams are about 3 mm. The counter-propagating probe beam overlaps with the pump beam inside the Rb vapor cell and is detected by a Si PIN photodiode

#153748 - $15.00 USD Received 30 Aug 2011; revised 5 Oct 2011; accepted 5 Oct 2011; published 2 Nov 2011

with a bandwidth of 12.5 MHz. The detected signal is demodulated by an rf mixer after passing through a 5-MHz low pass filter. The IF output of the mixer is filtered by a 30-kHz low pass filter, and observed using an oscilloscope. We use a two channel signal generator as the local oscillator to control the modulation index and the detector phase. The two outputs are internally phase-locked to a common reference oscillator. Therefore, we can precisely control the relative phase between the two 3 MHz outputs. One of the outputs drives the EOM to control the modulation index, and the other output is injected into the LO port of a mixer to control the reference phase.

4. Results

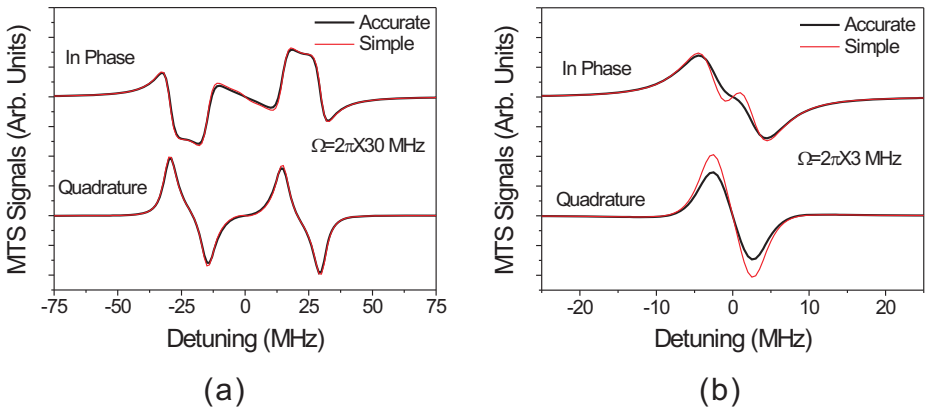

Fig. 2. The MTS signals for two-level atoms at the modulation frequency of (a) $\Omega/(2\pi)$ = 30 MHz and (b) $\Omega/(2\pi)$ = 3 MHz.

Figure 2 shows the calculated results for two-level atoms to verify the validity of the approximation of using only three oscillation frequencies for the populations, not the 11 frequencies as reported in Ref. [14]. Figures 2(a) and 2(b) show the MTS signals (in-phase and quadrature) at a modulation frequency $\Omega/(2\pi)$ of 30 MHz and 3 MHz, respectively. We assumed that the Rabi frequencies of the carrier, sideband, and the probe beams are $\Omega_c = 0.5\Gamma$, $\Omega_s = 0.25\Gamma$, and $\Omega_p = 0.5\Gamma$, respectively, and the laser beam diameter is 3 mm. We can see a good agreement between the accurate and approximate results at $\Omega/(2\pi) = 30$ MHz in Fig. 2(a). In contrast, there exits a slight discrepancy in Fig. 2(b) at $\Omega/(2\pi) = 3$ MHz. However, this can be neglected when calculations are performed for real ^{87}Rb atoms because the main aim of the calculation is to obtain an approximate lineshape of the MTS spectra for real atoms.

Now we discuss the results for the ^{87}Rb atoms. Figures 3(a) and 3(b) show the calculated and experimental results of the MTS signals, respectively, for the transitions $F_g = 2 \rightarrow F_e = 1,2,3$, i.e., for transitions from the upper ground state ($F_g = 2$). The Rabi frequencies of the carrier, sideband, and probe beams are $\Omega_c = 0.5\Gamma$, $\Omega_s = 0.25\Gamma$, and $\Omega_p = 0.5\Gamma$, respectively, where the decay rate of the excited state is $\Gamma = 2\pi \times 6.065$ MHz [17]. We used rather strong probe beam's intensity because we observed weak MTS signal when Ω_p was smaller than 0.5Γ. The modulation frequency is $\Omega/(2\pi) = 3$ MHz. The comparison of experimental and calculated results for other modulation frequencies is to be investigated. The diameter of the laser beams is about 3 mm. From the top of the figures, the in-phase and quadrature components of the MTS spectra are plotted. The saturated absorption spectroscopy (SAS) spectrum is displayed in order to identify the frequencies in Fig. 3(a). In the SAS spectrum, S_μ represents the resonance signal

#153748 - $15.00 USD Received 30 Aug 2011; revised 5 Oct 2011; accepted 5 Oct 2011; published 2 Nov 2011

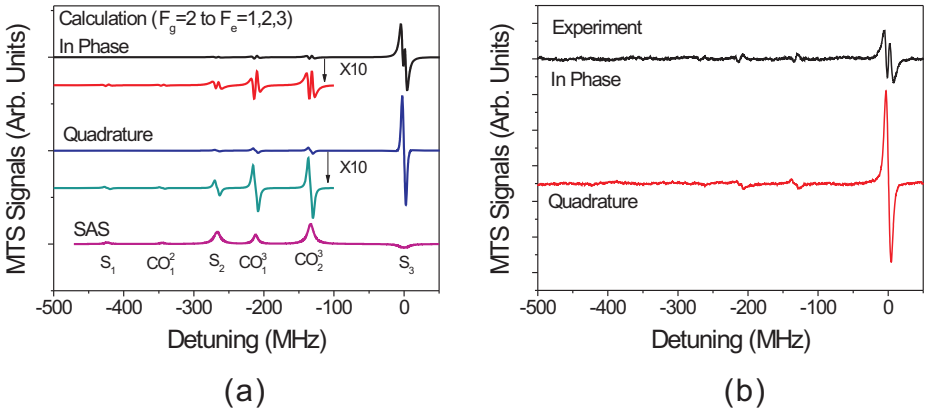

Fig. 3. (a) The calculated and (b) experimental results of the MTS spectra for the transitions $F_g = 2 \rightarrow F_e = 1, 2, 3$ of ^{87}Rb atoms.

for the transition $F_g = 2 \rightarrow F_e = \mu$, and C_μ^ν denotes the crossover signal related to the transitions $F_g = 2 \rightarrow F_e = \mu$ and $F_e = \nu$. In Fig. 3(a), in order to see the signals other than the dominant signal corresponding to the cycling transition $F_g = 2 \rightarrow F_e = 3$, the spectra are expanded by a factor of ten and are displayed just below the whole spectra.

It can be clearly seen that there exist three resonance signals and three crossover signals as in the SAS spectrum. In addition, we can see that the resonance signal for the cycling transition is very large and is approximately ten times bigger than the other signals. As explained in a previous report [14], the large signal for the cycling transition line is attributed to long interaction time of the atoms with the laser beam. We also found that the crossover signals where the cycling transition line is involved (C_1^3 and C_2^3) are much larger than the other crossover signal (C_1^2). In Figs. 3(a) and 3(b), we can see good agreement between the calculated and experimental MTS spectra. The dispersive MTS signal for the quadrature component can be used for laser frequency stabilization. In contrast, it is necessary to use a smaller modulation frequency to achieve a dispersive in-phase component in the MTS signal.

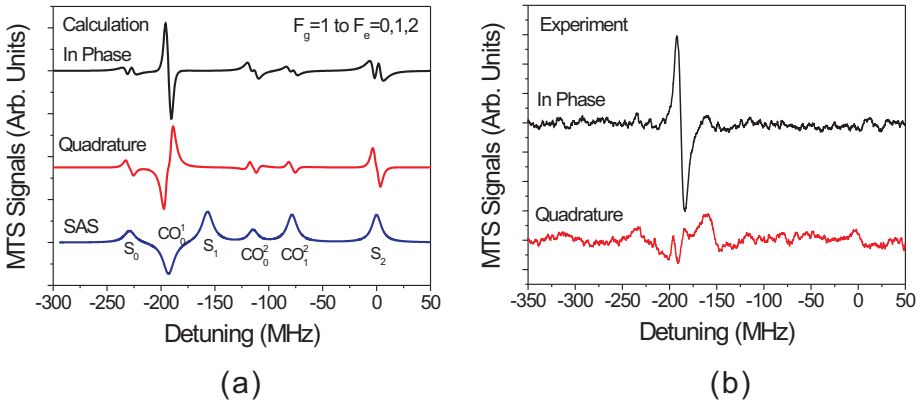

Fig. 4. (a) The calculated and (b) experimental results of the MTS spectra for the transitions $F_g = 1 \rightarrow F_e = 0, 1, 2$ of ^{87}Rb atoms.

#153748 - $15.00 USD Received 30 Aug 2011; revised 5 Oct 2011; accepted 5 Oct 2011; published 2 Nov 2011

The calculated and experimental results for the transitions from the lower ground state ($F_g = 1$), i.e., for the transitions $F_g = 1 \rightarrow F_e = 0, 1, 2$, are shown in Figs. 4(a) and 4(b), respectively. As is in Fig. 3, the in-phase and quadrature components of the MTS signals, and SAS spectrum are plotted from the top of the panel. The parameters are the same as those used in Fig. 3. Comparing the calculated and experimental results, we observe a good agreement for the in-phase components of the MTS signal. We also see a large dispersive signal for the crossover line (CO_0^1). In contrast, the relatively large signal of the calculated quadrature component for the crossover line (CO_0^1) is not striking in the experimental result. We find that the MTS signal for the transitions from the lower ground state is strongly dependent on the various parameters used such as the Rabi frequencies and beam diameter. Therefore, the discrepancy observed in the MTS signal for these transitions may be due to inaccurate measurement of experimental parameters. Further detailed study, including looking into the polarization dependence for these transitions, is scheduled for the near future.

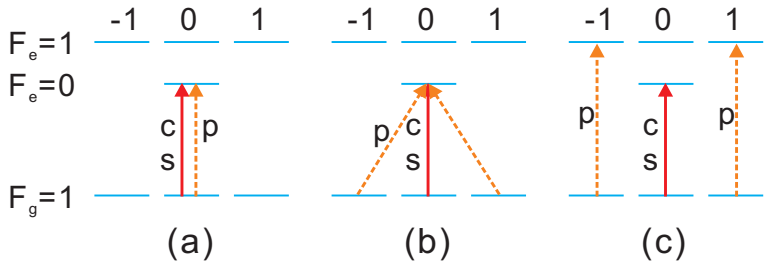

Fig. 5. Energy level diagrams for the transitions $F_g = 1 \rightarrow F_e = 0$ where the linearly polarized carrier (c) and sideband (s) beams are (a) in parallel and (b) perpendicular to the linearly polarized probe beam (p). (c) Diagram for the crossover signal (CO_0^1).

In contrast to the results in Fig. 3, we have three salient characteristics of note in the results seen in Fig. 4: one is the disappearance of the resonance signal for the cycling transition $F_g = 1 \rightarrow F_e = 0$, the second is the appearance of the large MTS signal for the crossover line (CO_0^1), and the third is the disappearance of the signal for the transition $F_g = 1 \rightarrow F_e = 1$. We might expect that the signal for the transition $F_g = 1 \rightarrow F_e = 0$ to be large because this transition is cycling like the transition $F_g = 2 \rightarrow F_e = 3$. However, we did not observe a large signal for this transition in practice. This is because the polarizations of the beams are all linear. As shown in Fig. 5(a), the population in the ground state $|F_g = 1, m_g = 0\rangle$ is optically pumped to the states $|F_g = 1, m_g = \pm 1\rangle$. Although this transition is cycling, because the population of the state $|F_g = 1, m_g = 0\rangle$, which would contribute to the MTS signal in this polarization configuration, decreases, a weak MTS signal is obtained. Therefore, as shown in Fig. 5(b), we expect a large signal for other polarization configurations such as linear polarizations with a perpendicular direction.

The second characteristic, the appearance of the large MTS signal for the crossover line (CO_0^1), can be understood by the scheme shown in Fig. 5(c), where the carrier and the sidebands are tuned to the cycling transition $F_g = 1 \rightarrow F_e = 0$, while the probe beam is tuned to the transition $F_g = 1 \rightarrow F_e = 1$. Atoms can be optically pumped to $|F_g = 1, m_g = \pm 1\rangle$ by the carrier and the sideband beams. Then, the MTS signal can be generated by the atoms at $|F_g = 1, m_g = \pm 1\rangle$, although the populations in those states decrease monotonically due to optical pumping.

The third characteristic, the disappearance of the signal for the transition $F_g = 1 \rightarrow F_e = 1$, originates from the fact that the transition strength between the states $|F_g = 1, m_g = 0\rangle$ and $|F_e = 1, m_e = 0\rangle$ vanishes. When the frequency of the linearly polarized light is tuned near the transition $F_g = 1 \rightarrow F_e = 1$, the population is optically pumped to the state $|F_g = 1, m_g = 0\rangle$. As

#153748 - $15.00 USD Received 30 Aug 2011; revised 5 Oct 2011; accepted 5 Oct 2011; published 2 Nov 2011

the state $\left|F_g = 1, m_g = 0\right\rangle$ is not able to connect to the excited state, the signal for this transition line can not be observed. If other polarization configurations are used, we may expect a signal for this transition.

5. Conclusions

In this paper we presented a theoretical and experimental study of lineshape in modulation transfer spectroscopy for ^{87}Rb atoms. Although many studies of MTS for real atoms have been published, detailed theoretical calculations for real atoms have not been performed to the best of our knowledge. We calculated MTS spectra for ^{87}Rb atoms by solving the complete time-dependent optical Bloch equations without the use of any phenomenological constants. As can be expected from the calculation for two-level atoms, we observed a large dispersive signal for the cycling transition line from the upper ground state ($F_g = 2$). This large signal results from the long interaction time between the atoms and the laser light. We also compared the calculated results with experimental results and found good agreement. In contrast, for the transitions from the lower ground state ($F_g = 1$), we observed a large signal at the crossover line (CO_0^1) and weak signal at the resonance cycling transition line ($F_g = 1 \rightarrow F_e = 0$). These occur because of the linear laser polarizations which are all in parallel. Since the MTS signals for the transitions from the lower ground state seemed to be strongly dependent on the laser polarizations, we are currently studying the dependence of the signals on the laser polarization. The method of calculation developed in this paper is generally applicable to other nonlinear optical phenomena where several frequencies are involved, such as multiwave mixing in an atomic vapor.

Acknowledgments

This research was supported by Basic Science Research Program through the National Research Foundation of Korea(NRF) funded by the Ministry of Education, Science and Technology(2011-0009886).

#153748 - $15.00 USD Received 30 Aug 2011; revised 5 Oct 2011; accepted 5 Oct 2011; published 2 Nov 2011